Available online at www.sciencedirect.com

ScienceDirect

Current Opinion in Electrochemistry

Review Article

Structural and electrochemical heterogeneities of boron-doped diamond surfaces

Robert Bogdanowicz and Jacek Ryl

Abstract

This brief review is focussed on the recent progress in studies of the heterogeneous electrochemical behaviour of various boron-doped materials extending from zero-dimensional particles through polycrystalline or nanostructured three-dimensional surfaces. A boron-doped diamond reveals large heterogeneities induced by numerous factors, *inter alia* multi-faceted crystallinity, inhomogeneous boron concentration, sp^2/sp^3-carbon ratio, surface terminations and grain size distribution. We also present single nanodiamond particles and a nanostructured diamond, which are fabricated by either a top-down or a bottom-up procedure. Nanoarchitectured surfaces allow high areas and large aspect ratios to be achieved, exhibiting highly heterogeneous charge-transfer performance for catalytic, sensing and energy applications. We have anticipated multi-factor-originated heterogeneities of various boron-doped diamond surfaces displaying the essential fabrication and diagnostic methodologies and critically reviewing their benefits and drawbacks.

Addresses

Gdańsk University of Technology, 11/12 Gabriela Narutowicza Street, 80-233 Gdańsk, Poland

Corresponding author: Bogdanowicz, Robert (rbogdan@eti.pg.edu.pl)

Current Opinion in Electrochemistry 2022, **31**:100876

This review comes from a themed issue on **Diamond Electrochemistry**

Edited by **Guohua Zhao, Nianjun Yang, Carlos A. Martínez-Huitle**

For a complete overview see the Issue and the Editorial

Available online 3 November 2021

https://doi.org/10.1016/j.coelec.2021.100876

Keywords

Diamond, Boron-doped diamond, Nanodiamond, Heterogeneous transfer rate, Mapping, SECM.

Introduction

Diamond is a unique material that competes strongly with various semiconductor materials, thanks to its extraordinary physicochemical and electronic performance. The doping of diamond by boron results in the formation of hole conductivity with an activation energy of 0.36 eV [1]. Boron-doped diamond (BDD) is known for its extraordinary electrochemical performance, including a wide electrolytic window of approximately 3.5 V, low background currents, stability in harsh environments and biocompatibility [2]. Those properties opened the way to systematic studies focussed on a variety of approaches in electroanalytical applications, water purification issues, electrosynthesis and electrochemical energy storage and conversion. Most synthetic diamond structures are multi-faceted and polycrystalline due to the nature of their fabrication utilising particularly high-pressure high-temperature or chemical vapour deposition (CVD) [1,2]. The incorporation of boron as a dopant generally in the range of 10^{16}–10^{22} atoms cm^{-3} considerably affects the electronic properties, impurities, molecular structure and composition of the crystallographic facets of diamond. Various boron incorporations in the particular facet, sp^2/sp^3-carbon ratio, sp^2 impurities and specific surface terminations of selected orientations (i.e. hydrogen or oxygen groups) are the key factors provoking electrochemical heterogeneities. Nevertheless, diamond terminations could be explicitly altered by the large variety of developed strategies involving such processes as thermal, plasma, electrochemical, chemical or photochemical treatments [1,3]. The achieved functionality tunes the distribution of surface termination and the magnitude of its electrochemical heterogeneity. Furthermore, the complex characters of numerous diamond-built architectures reveal various heterogeneous electrochemical behaviours that are dependent on their dimensions scaled from nearly zero-dimensional single particles along multi-faceted surfaces up to 3D-sculptured nanostructures (see Figure 1 and Table 1). Besides the widely studied multi-faceted BDD surfaces, single nanodiamond (ND) particles have recently attracted the attention of scientists, thanks to their versatile diamond nature supplied by a highly active area, large aspect ratios and surficial groups or boron-induced electroactivity [4–6]. The lateral homoepitaxial mechanism allows the formation of zero-dimensional nanoparticles or 3D-architectured nanowires [7] with large aspect ratios that exhibit directional charge-transfer performance. The flexible C–C surface chemistry along with nanostructuring (top-down or bottom-up) of conductive diamond surfaces results in enhanced heterogeneous wetting and

Figure 1

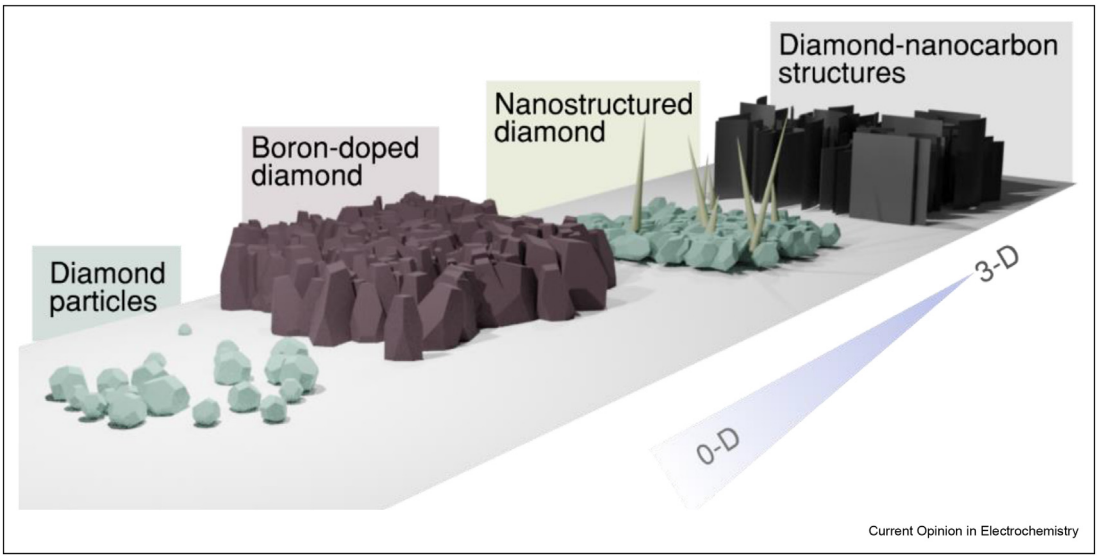

Overview of multi-dimensional diamond-built architectures highlighted in this work, revealing heterogeneous electrochemical behaviour.

electronic properties, catalytic activity and electrochemical performance for sensing and energy applications [8].

Furthermore, a large variety of electrochemical diamond-based devices have manifested as valuable materials for, *inter alia*, supercapacitors [9,10], pharmaceutical sensing [11], detection of food compounds [12] and electroanalysis of biomolecules [13–15]. Importantly, a few works have reported a significant impact of sp^2-carbon impurities on the electrochemical kinetics modulating the heterogeneous electron transfer (HET) rate of specific redox couples [16–18].

Consequently, we focussed this mini-review on the very recent progress in the heterogeneous electrochemical behaviour of a large variety of boron-doped materials spreading from almost zero-dimensional particles through multi-faceted surfaces to nanoarchitectured three-dimensional structures. We have anticipated multi-factor-originated heterogeneities tuned by the geometric, physicochemical and electronic properties of diamond, displaying the essential methodologies and critically reviewing their benefits and drawbacks.

Facet-induced electrochemical performance of nanodiamond particles

A framework of functionalised nanodiamond particles was manifested by Duan et al. [6] as carbocatalysts displaying diverse heterogeneous reactions. *In-situ* B- and N-codoping of diamond forms nanoscale-interacting hybrid particles, which tend to aggregate due to the high surface energy. The B/N co-doped ND crystals display an upshifted positive potential peak along with the high current density ($\sim$51 mA cm^{-2}) of a four-electron oxygen reduction reaction (ORR). The formation of microsized single-diamond particles by a high-pressure and high-temperature (HPHT) process has been recently reported by Wang et al. [19]. The formed large diamond crystals are dominated by (111) facets because the HPHT growth is driven by small nanocrystals adsorbed to larger seeds in a metal matrix that minimises their surficial energy. An analogous approach was utilised by Wood et al. [20] for the synthesis of boron-doped microparticles utilising AlB_2 as a solid-state precursor. Figure 2(g–h) displays FE-SEM images of a polished surface of the HPHT-compressed boron-doped particles ((111)-dominant planes) fabricated with two different dopant concentrations providing metal-like conductivity. The polished surface is dominated by (111) planes (see Figure 2(i)) that exhibit void-induced porosity and a low level of sp^2-carbon impurities, increasing the current magnitudes in the reduction range (see Figure 2(j)). Figure 2(k) shows scanning electrochemical microscopy (SECM) maps with relevant cyclic voltammetry (CV) curves, which exhibit a heterogeneous nature with negligible dependence on the specific crystallographic facet, thanks to the uniform boron dopant concentration. The high-rate CVs were obtained at a resin-isolated (111)-faceted surface using a nanopipette in 10 mM $Ru(NH_3)_6Cl_3$ and 10 mM KNO_3 electrolyte (see Figure 2(l) with FE-SEM of the isolated (111) plane in the inset) with an increased double-layer capacitance of approximately three orders of magnitude concerning the planar CVD-grown BDD.

The CVD enables the growth of free-standing microsized H-BDD crystals containing (100) and (111) facets (see Figure 2(a–b)) when a very low seeding density is applied [5]. The SECM data revealed large

Table 1

Summary of heterogeneous electrochemical properties of BDD surfaces.

Diamond type	Electrochemical performance	Studied application	Crystallinity	Heterogeneities origin	Ref.
MW-CVD-grown BDD	termination-based electron kinetics	pre-treatment assessment	multi-faceted	grain structure, surface termination, treatment procedure	[3,41]
CVD-grown nanodiamonds	low currents, fast electron kinetics	n/a	(100) and (111)	surface termination, boron distribution	[5]
MW-CVD-grown BDD	heavy B-doped, high kinetics	DEFB1 gene recognition	multi-faceted	effective DNA at BDD hybridisation	[15]
Graphite@heavily doped BDD	enhanced LOD and stability	acetaminophen detection	multi-faceted, (111) facets affected	sp^2-carbon thin films, crystallinity	[17]
MPCVD-grown BDD spheres	long-term stability	AFM probes, organics sensor	polycrystalline	probe polarity, surface termination	[29]
MW-CVD-grown BDD	altered currents and electrolytic window	electrocatalytic, OER	(110) with minor (100) contribution	boron distribution, surface termination	[39]
Core–shell D/G nanoarchitecture	enhanced electron kinetics, small ΔE	Pb^{2+}, Cd^{2+} and Zn^{2+} detection	(111) diamond and (002) graphite	sp^3/sp^2 ratio	[40]
HPDG on SCD	termination-based Schottky contact	electronic devices	(100) and polycrystalline	HPDG structure, surface termination	[21]
MPCVD-grown low-doped BDD	decrease with sp^2 content increase	n/a	polycrystalline, primarily (111)	sp^2-carbon content	[50]
porous BDD at SiO_2 nanofibres	enhanced electron transfer rates	dopamine detection	polycrystalline	sp^2-carbon content, porosity	[51]
HPHT compacted microdiamonds	high currents, fast electron kinetics	n/a	(111)	porosity	[20]
ND at the BDD surface	high currents, fast electron kinetics	n/a	multi-faceted	sp^2-carbon impurities, grain size distribution	[22]

heterogeneities of $K_4[Fe(CN)_6]$ electron transfer induced by a selected crystalline facet as displayed in Figure 2(c). The spatially resolved i–E studies of BDD particles (see Figure 2(d)) manifested that the (111) planes drive faster electron transfer kinetics, thanks to the higher boron level *in-situ* incorporated during the CVD process. The (111)-oriented facets at the O-BDD surface (blue curve in Figure 2(e–f)) demonstrated impaired electron transfer kinetics versus an H-terminated surface (red curve in Figure 2(e–f)) ascribed to the electronic properties (i.e. lower conductivity and carrier densities). This effect is suppressed at oxidised (100)-planes due to the initial low concentration of charge carriers, where faradaic currents were undetectable. A valuable insight into local surface termination-dependent BDD conductivity was presented by Wang et al. [21], who studied hill-like polycrystalline diamond grains (HPDG) randomly emerging on heavy boron-doped p+ single-crystal diamonds (SCD).

Gupta et al. [22] reported that a drop-cast ND at a BDD surface supports electrocatalytic processes due to the domination of surface states as acceptors. The SECM mapping of this hybrid surface displays highly electroactive 'hot spots' attributed to the core–shell nanodiamond–BDD interfaces and the sharp edge-planed sites of ultrasonically deagglomerated nanodiamond particles. Pleskov et al. [23] developed BDD compacts introducing a catalytically active metal, platinum, in the course of metal growth. These are prepared in high temperature and pressure, but unlike HPHT, single crystals have grown without the seed-crystal representing a submicron-sized compact mass of diamond crystallites. These compacts were verified to show high electroactivity concerning an anodic chlorine evolution reaction, while the structural homogeneity is affected by the presence of well-distributed Pt subsurface inclusions and pits, both micrometre-sized. Next, synergistic electrocatalytic CO_2 reduction to C_2 species was observed at the heterogeneous nitrogen-doped nanodiamond/Cu interface [24]. Copper-stabilised nanodiamond surfaces manifested more than 60% of faradaic efficiency towards C_2; its incorporation produced a catalytic effect, decreasing the CO_2 overpotential of bare nitrogen-doped diamonds.

Finally, the first-principles approach allowed for the atomic-scale understanding of the orientation and dopant concentration-dependent electronic band-structure of BDD surfaces observed as a variation of the energy-impacted electronic density of states [25]. The main parameters affect the experimentally observed, faced-induced BDD heterogeneities. Simulation of electronic transport exhibited a distinct impact of the boron dopant on the (111) facet, where it decreased carrier mobility. Those results indicated that the

Figure 2

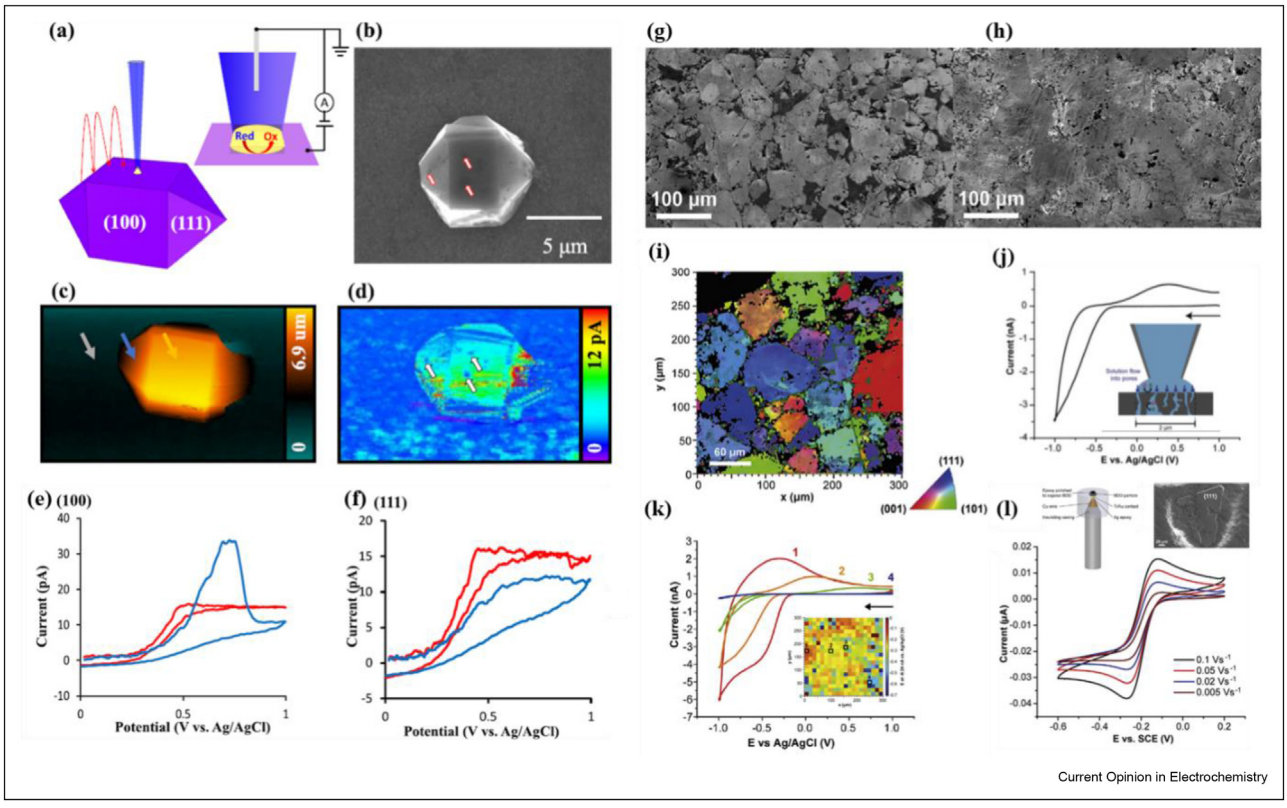

Overview of facet-induced electrochemical performance of nanodiamond particles. **(a)** Scheme of the SECM conducted at an H-BDD single particle; **(b)** SEM of a (100)-facet H-BDD particle; **(c)** SECM topography and **(d)** current imaging of an H-BDD single particle with the (100) and (111) facets; **(e, f)** CV recorded at (100) and (111) facets of H/O-BDD. Reproduced with permission from Ref. [5] (DOI: *10.1021/acs.analchem.1c00053*). Copyright 2021, American Chemical Society. FE-SEM of nanodiamond electrodes fabricated using HPHT BDD particles mixed with 3.6 wt.% AlB_2 **(g)** and 4.8 wt.% AlB_2 **(h)**; **(i)** EBSD image and **(j)** CV measured at the (111) facet of a sample of 4.8 wt.% AlB_2 HPHT BDD along with a schematic representation of an electrode/electrolyte interface in the inset; **(k)** CVs and map of onset potentials of the SECCM scan area on 4.8 wt.% AlB_2 HPHT BDD; **(l)** CVs of SPE recorded in 1 mM $Ru(NH_3)_6^{3+/2+}$ (inset: design of the HPHT BDD SPE; SEM image of a (111)-faceted HPHT BDD particle masked with epoxy resin). Reproduced with permission from Ref. [20] (DOI: *10.1016/j.carbon.2020.09.038*). Copyright 2021, Elsevier.

frustrating transition of insulator to metal occurred on the (110) surface, while the (111) surface revealed a re-entrant transition from insulator to metal behaviour [26].

Mapping of electrochemical heterogeneities of BDD surfaces

Numerous surface-resolved methods have already been developed to obtain information on local changes in electrochemical activity or physicochemical/electronic properties directly related to reduction/oxidation reactions. Microscopic techniques such as SECM [27,28], scanning probe microscopy (SPM) [3,29] and local electrochemical impedance spectroscopy (LEIS) [30] are commonly utilised to investigate the electrochemical processes that occurred at heterogeneous, micro- and nanostructured surfaces [31]. Nanostructured ultramicroelectrodes (UME) [32,33] enable the investigation of single-molecule processes in complex media, delivering insight into the understanding of the relation between a specific subsurface element (i.e. facet, pore, defect or impurity) and the single electrochemical entity. Colloidal AFM probes with a micrometre-sized BDD sphere attached to a cantilever offer significant enhancement of the mechanical properties and abrasion resistance even after multiple scans with unprecedented spatial resolution [29]. Furthermore, due to BDD's excellent electrochemical properties, these probes may be used for hybrid AFM-SECM devices in an electrolytic environment. Depending on the BDD termination type, the interaction with other surfaces, solvents and molecules may be altered, enhancing the quality of chemical imaging [34]. Furthermore, the combination of plasmon-based optical and electrochemical methodologies results in synergistic and remote studies revealing enhanced information on the spatially resolved molecular level electrochemistry or single nanoparticle catalysis supported with charge transport data with sub-nanometric resolution [35].

Nanoscopic electrochemical scanning probe microscopy (EC-SPM) techniques [36] allow the redox and

electrocatalytic properties to be mapped. Henrotte et al. [37] studied the electrocatalytic ORR activity using BDD as the substrate for the catalyst, for which the total O_2 consumption was obtained before O_2 consumption started at the BDD, proving the ability to investigate very low electrolytic activities. SECM was also used to study the pH differences resulting from the appearance of water oxidation products, allowing the formation of multiple intermediates affecting the kinetics at the BDD surface to be distinguished [38]. The authors revealed how the evolution of water splitting products is bound to a localised drop in the HET rate, a feature connected with regions of pure diamond and sp^2-carbon phase. Binding SECM with CV measurements at each pixel showed that the electrolytic potential of polycrystalline BDD is directly linked to the local boron dopant concentration and increases in more doped facets [39] (see Figure 3(a–d)). Moreover, the sensitivity of the onset potential changes primarily for the hydrogen-terminated (H-BDD) electrodes, while spatial heterogeneities were observed only at the most extreme polarisation potentials for oxygen-terminated (O-BDD) surfaces.

BDD oxidation selectivity [41] originates from the local differences in the facets of boron doping. Here, the SECM studies were supported by multi-sine impedimetric techniques: nanoscale impedance microscopy (m-NIM) and dynamic electrochemical impedance spectroscopy (DEIS). The propensity towards BDD surface oxidation was related to crystallographic orientation while small differences in polarisation conditions lead to a significant change in the BDD thin-film electrode response. The use of m-NIM proved a correlation between different levels of electric heterogeneity and the O-BDD modification method, see Figure 3(e–h) [3]. The m-NIM was found to be the most efficient tool to precisely define the O-BDD transition compared to XPS and contact angle analyses. The most prominent surface resistance heterogeneity was observed for heating in air at 600 °C. This treatment in particular may affect the electrochemical performance, modifying the distribution of local diffusion fields but also leading to degradation of the grain structure under prolonged exposure [42]. It became evident that certain crystallographic planes are more prone to surface oxidation and etching, in particular

Figure 3

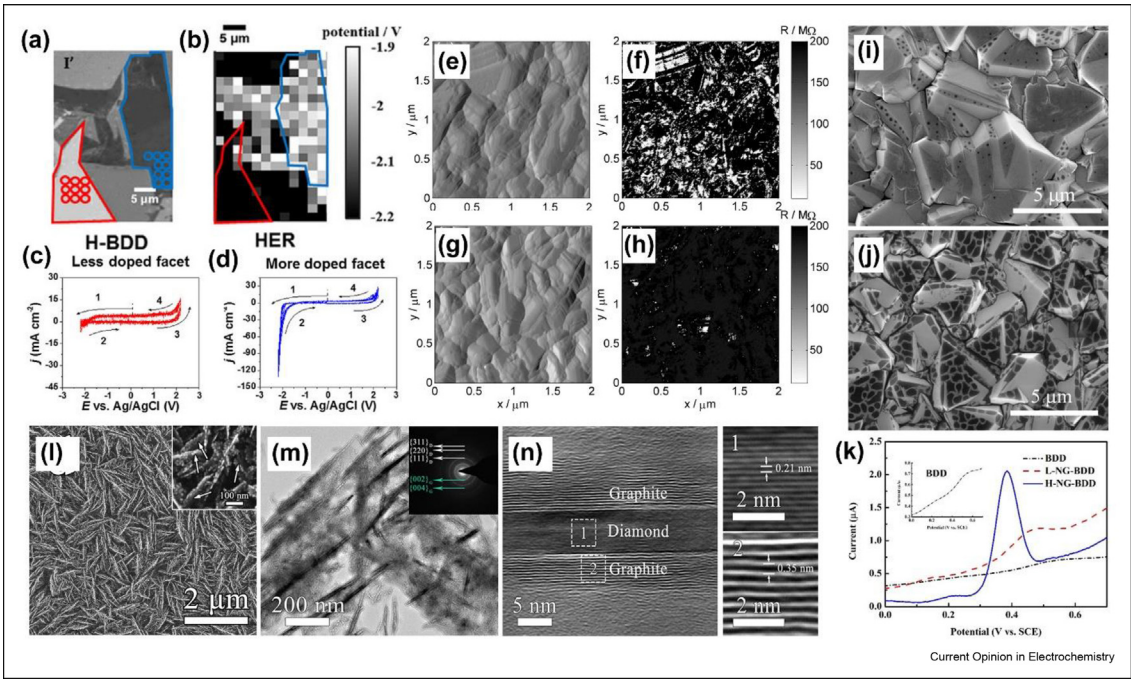

SEM image of polycrystalline BDD **(a)** with corresponding SECM onset cathodic potential image for a current density of –3.5 mA cm^{-2} **(b)** and corresponding CVs for a less doped facet (red circles in (a)) **(c)** and a more doped facet (blue circles in (a)) **(d)**. Reproduced with permission from Ref. [39] (DOI: *10.1002/celc.201800770*). Copyright 2018, Chemistry Europe. O-BDD surface oxidised when exposed to 600 °C in the air **(e,f)** and oxygen plasma and a 50 W UV lamp **(g,h)**, AFM contour micrographs **(e,g)** and corresponding m-NIM surface resistance maps **(f,h)**. Reproduced with permission from Ref. [3] (DOI: *10.1016/j.ultramic.2019.01.004*). Copyright 2019, Elsevier. SEM images of NG-BDD films grown at 950 °C **(i)** and 1050 °C **(j)**, with corresponding DNPV curves **(k)** for 6.5 μM acetaminophen obtained on these electrodes in 0.1 M PBS at a scan rate of 50 mV s^{-1}. Reproduced with permission from Ref. [17] (DOI: *10.1021/acsomega.0c06141*). Copyright 2021, American Chemical Society. SEM morphology of diamond–graphite films grown with a 12% CH_4 gas mixture (inset: arrows indicate nanoplatelet-like grains) **(l)**, with low-magnification (inset: corresponding SAED patterns) **(m)** and HRTEM **(n)** images of these films. Right panels exhibit magnified HRTEM images corresponding to the dashed rectangles in the left parts. Reproduced with permission from Ref. [40] (DOI: *10.1021/acs.jpcc.8b11865*). Copyright 2021, American Chemical Society.

(111) facets. The influence of surface orientation on the electrochemical properties of the BDD thin-film electrodes was investigated by Ivandini et al. [43], who performed studies on (100) and (111) homoepitaxial single-crystal and polycrystalline BDD surfaces. Their studies found that the (111) plane was more reactive, a feature visible regardless of the termination type, yet enhanced for O-BDD surfaces. Moreover, the authors' XPS reports show that (100) surfaces are more prone to selective oxidation compared to (111) surfaces. Interestingly, the polycrystalline BDD electroactivity was the highest, most likely due to the heterogeneity of boron distribution [41]. Electrochemical pre-treatment and polishing enhance the electroanalytical performance of BDD surfaces, increasing their electrochemically active surface area (EASA) which offers lower limits of detection or a wider range of linearity [44]. BDD film anodes reveal outstanding performance in electro-Fenton processes, enhancing the electrolysis of pollutants [45]. BDD anodes were also widely tested towards electrochemical disinfection of bacteria [46]. BDD surfaces reveal high mineralisation efficiency depending on the generation of hydroxyl radicals, the local concentration of which tends to be highly heterogeneous, which together with high fabrication costs limits the large-scale applications [47,48].

Efficient BDD-based biosensors were reported after surface modification of (111) facets of BDD by converting the diamond structure to sp^2-carbon at high temperatures [17]. Boron doping plays a key role in the temperature-driven BDD modification, which is also presumable the reason why (111) facets of BDD are favourably affected. These nanometre-sized graphite-BDD films (NG-BDD) were then used to detect trace amounts of acetaminophen with limits of detection (LOD) ranging to 5 nM when the film was grown in 1050 °C, see Figure 3(i–k). On the other hand, substitution of hydrogen with deuterium during BDD growth enhances the electrochemical properties, increasing the boron doping and share of (111)-oriented crystals and decreasing the non-diamond sp^2 phase contribution [49]. The reported boron dopant concentration under the same MW PACVD conditions was nearly two orders higher. This material possesses exceptionally high electrochemical performance, featuring 61 mV peak separation in a CV experiment (at 5 mV s^{-1}), nearly 4× lower charge-transfer resistance, and as a result, a very low paracetamol LOD (0.76 μM). Niedzialkowski et al. [15] monitored electrode heterogeneity and detected the presence of the human-specific DEFB1 gene in samples collected from saliva extracts. The detection was possible by tracking the impedance at the charge-up electrode surface, through subtle geometry changes of anchored hybridised DNA.

It is commonly accepted that the electrochemical performance of BDD increases with the increased boron doping concentration. However, an opposite tendency was reported by Xu et al. [50] for low-doped BDD thin-film electrodes (0.1% and 1% boron in the gas mixture were tested). Baluchová et al. [51] compared planar electrodes with layers grown on SiO_2 nanofibres, to study the influence of the surface development on the electrochemical characteristics of BDD. Unlike planar BDD, the higher sp^2-carbon content in porous BDD was found to affect the electrochemical performance more than the boron doping level. The peak separation in CV studies was reported as low as 30 mV for porous electrodes, bound with adsorption of the redox probe in the porous material, and a contribution from thin-layer diffusion. Enhanced electron transfer rates result in higher sensitivity for dopamine sensing, reaching 0.21 μM.

The few recently published reports on BDD-based supercapacitors reveal the influence of the nanostructured diamond surface. Zhang et al. [52] exhibited excellent capacitive performance of BDD after reactive-ion etching (RIE) in an oxygen plasma, leading to the formation of nanospikes (up to 280 nm high) greatly enhancing the specific surface area. Longer nanospikes are formed after a longer RIE process duration, but a 5 min etch was optimal to avoid exfoliation. These O-BDD surfaces possess a high specific capacity of 70.6 mF cm^{-2} (at 0.32 mA cm^{-2}) with a capacitance retention of 84.3% after 15k cycles in galvanostatic charge/discharge (GCD) tests. Nanospikes were also grown directly on BDD by Banerjee et al. [53] in a gas admixture containing B_2H_6 and N_2. These structures were composed of up to 63% of the sp^2-carbon phase, based on XPS findings. As a result, the electrode topography is intriguing, with cauliflower-like grains and rising spikes that have an average height of nearly 2 μm and a bottom thickness reaching 100 nm. The electrodes are reported to possess a specific capacitance of 250 mF cm^{-2} (at 3 mA cm^{-2}) and 77.8% capacitance retention after 164 h of GCD tests. A symmetric capacitor built with BDD grown on titania nanotubes and operating in an aqueous electrolyte was characterised by 15 mF cm^{-2} capacitance, 24.68 kW kg^{-1} power density and 93% retention after 100k GCD cycles [10]. The remarkable characteristics of the material were delivered by nanoporous, multi-faceted and substoichiometric TiC, forming clusters at the lateral surfaces of the titania nanotubes. Manipulating the methane concentrations during film growth leads to the formation of diamond–graphite nanoplatelets, exceeding 8% CH_4 in a gas mixture [40]. The formation of conductive nanostructures decreased the working electrolytic window and increased the double-layer capacitance, also lowering the peak-to-peak separation in CV studies. The HRTEM demonstrated the nanoplatelets to possess a core–shell structure, with diamond grains surrounded by a 4 nm thick graphite layer, while the interplanar distances suggested (111) diamond and (002) graphite facets, see Figure 3(l–n).

Similar hybrid diamond—graphite nanoplatelet surfaces were studied by Santos et al. [54], demonstrating superficial heterogeneous faradaic charge transfer between these facets. The nanodiamond platelets deliver enhanced electron transfer rates improving the electroactivity of the nanographitic cores.

Summary and future perspectives

Summarising, this brief review presents the recent progress in studies concerning structural and chemical modifications of a large variety of BDD derivatives, introducing the heterogeneous electrochemical behaviour and thus affecting the key properties of diamond materials. We also present the trends in mapping the local electric heterogeneity, including SECM, SPM and other techniques. We have anticipated multi-factor-originated heterogeneities tuned by geometric, physicochemical and electronic properties of diamond displaying the essential fabrication and diagnostic methodologies and critically reviewing their benefits and drawbacks. Some examples of diamond types with various heterogeneities are summarised in Table 1.

Definitely, new technology has to be developed if we would like to go forward with broader BDD applications and improving its drawbacks such as inhomogeneities or heterogeneities. The current CVD and HPHT technologies have been developed and improved since the early 90s and their capabilities are practically exhausted in terms of hardware available on the market. A good chance of achieving a breakthrough in this area will be the development of a new technology or a significantly modified machine delivering homogeneous power to the growth surface over large areas (i.e. scaling a linear antenna system or DC arc plasma jet CVD).

The development of quantum modelling methods that give wider possibilities for the prediction of growth processes and selection of plasma parameters as well as interaction with the substrate could also push forward growth of a homogeneous diamond. The single-crystal diamond has so far only been achieved on the surface of monocrystalline iridium, but wider studies and other monocrystalline surfaces would probably allow for minimising heterogeneity by dominating a specific crystallographic phase, for example (111). Technologies for the synthesis of large single crystals, such as mosaic, are too expensive for broad electrochemical and electroanalytical applications, but advanced self-assembling nanodiamonds or microdiamonds with similar shapes might give a chance to obtain large homogeneous surfaces with a minor heterogeneity impact. New trends in the synthesis of diamond composites using HPHT with novel catalysts or novel approach applying a highly energetic plasma sintering are under development. Another aspect inducing heterogeneity is the nucleation and seeding utilised in CVD on non-diamond substrates. In this respect, further research on diamondoids or other molecular seeds as well as other diamond precursors, for example CCl_4 with a lower energetic barrier, would be desired. Furthermore, spatially selective modification of the BDD surface should be developed to minimise electrochemical heterogeneities through intelligent, targeted surficial grafting utilising for example metallic nanoparticles, nanodiamonds or conductive ceramics.

A nanoarchitectured diamond allows large aspect ratios to be achieved, often exhibiting a developed EASA and enhanced charge transfer for catalytic, sensing and energy applications. On the other hand, for the electroanalysis, the LOD and reproducibility depend on defining the initial state of the electrode, often uncontrollably affected by the electrochemical heterogeneities introduced together with surface modification procedures.

Author contributions

All authors have participated in (a) conception and design, or analysis and interpretation of the data; (b) drafting the article or revising it critically for important intellectual content; and (c) approval of the final version.

Declaration of competing interest

The authors declare that they have no known competing financial interests or personal relationships that could have appeared to influence the work reported in this paper.

Acknowledgements

This research work is supported by the Foundation for Polish Science under grant no. POIR.04.04.00-00-1644/18 and by the National Science Centre under SONATA BIS grant no. 2020/38/E/ST8/00409.

List of abbreviations

CVD	Chemical Vapour Deposition
DEIS	Dynamic Electrochemical Impedance Spectroscopy
DNPV	Differential Normal Pulse Voltammetry
EBSD	Electron Backscatter Diffraction
EC-SPM	Electrochemical Scanning Probe Microscopy
GCD	Galvanostatic Charge/Discharge
HET	Heterogeneous Electron Transfer
HPDG	Hill-like Polycrystalline Diamond Grains
HPHT	High-Pressure and High-Temperature
LEIS	Local Electrochemical Impedance Spectroscopy
m-NIM	Multi-frequency Nanoscale Impedance Microscopy
MW PACVD	Microwave Plasma-Assisted Chemical Vapour Deposition
OER	Oxygen Evolution Reaction
ORR	Oxygen Reduction Reaction
RIE	Reactive-Ion Etching

SAED	Selected Area Electron Diffraction
SCD	Single-Crystal Diamonds
SECCM	Scanning Electrochemical Cell Microscopy
SECM	Scanning Electrochemical Microscopy
SPE	Screen-Printed Electrode
SPM	Scanning Probe Microscopy
UME	Ultramicroelectrode

References

Papers of particular interest, published within the period of review, have been highlighted as:

* of special interest
** of outstanding interest

1. Yang N, Yu S, Macpherson JV, Einaga Y, Zhao H, Zhao G, Swain GM, Jiang X: **Conductive diamond: synthesis, properties, and electrochemical applications**. *Chem Soc Rev* 2019, **48**:157–204, https://doi.org/10.1039/C7CS00757D.

2. Nebel CE, Yang N, Yamasaki S: **Diamond: Carbon at its best**. *Carbon* 2021, **182**:711–714, https://doi.org/10.1016/j.carbon.2021.06.063.

3. * Zielinski A, Cieslik M, Sobaszek M, Bogdanowicz R, Darowicki K, Ryl J: **Multifrequency nanoscale impedance microscopy (m-NIM): a novel approach towards detection of selective and subtle modifications on the surface of polycrystalline boron-doped diamond electrodes**. *Ultramicroscopy* 2019, **199**:34–45, https://doi.org/10.1016/j.ultramic.2019.01.004.
The authors use an impedance-based SPM technique to evaluate spatial electric heterogeneities arising from O-BDD termination with different treatment procedures and originating from facets crystallinity.

4. Kumar S, Nehra M, Kedia D, Dilbaghi N, Tankeshwar K, Kim K-H: **Nanodiamonds: Emerging face of future nanotechnology**. *Carbon* 2019, **143**:678–699, https://doi.org/10.1016/j.carbon.2018.11.060.

5. ** Ando T, Asai K, Macpherson J, Einaga Y, Fukuma T, Takahashi Y: **Nanoscale reactivity mapping of a single-crystal boron-doped diamond particle**. *Anal Chem* 2021, **93**:5831–5838, https://doi.org/10.1021/acs.analchem.1c00053.
The spatially resolved i–E studies of free-standing microsized, CVD-grown H-BDD particles manifested that (111) planes drive faster electron transfer kinetics, thanks to the higher boron level *in-situ* incorporated during the CVD process. The (111)-oriented facets at the O-BDD surface demonstrated impaired electron transfer kinetics versus an H-terminated surface ascribed to the electronic properties.

6. Duan X, Tian W, Zhang H, Sun H, Ao Z, Shao Z, Wang S: **sp^2/sp^3 framework from diamond nanocrystals: a key bridge of carbonaceous structure to carbocatalysis**. *ACS Catal* 2019, **9**:7494–7519, https://doi.org/10.1021/acscatal.9b01565.

7. Wang Y, Wang W, Yang S, Shu G, Dai B, Zhu J: **Two extreme crystal size scales of diamonds, large single crystal and nanocrystal diamonds: synthesis, properties and their mutual transformation**. *N Carbon Mater* 2021, **36**:512–526, https://doi.org/10.1016/S1872-5805(21)60030-6.

8. Yang N, Zhao G, Foord J. *Nanocarbon electrochemistry*. 1st ed. Wiley; 2020, https://doi.org/10.1002/9781119468288.

9. Yang N. *Novel aspects of diamond*. Cham: Springer International Publishing; 2015, https://doi.org/10.1007/978-3-319-09834-0.

10. Bogdanowicz R, Dettlaff A, Skiba F, Trzcinski K, Szkoda M, Sobaszek M, Ficek M, Dec B, Macewicz L, Wyrębski K, Pasciak G, Geng D, Ignaczak A, Ryl J: **Enhanced charge storage mechanism and long-term cycling stability in diamondized titania nanocomposite supercapacitors operating in aqueous electrolytes**. *J Phys Chem C* 2020, **124**:15698–15712, https://doi.org/10.1021/acs.jpcc.0c02792.

11. Yence M, Cetinkaya A, Ozcelikay G, Kaya SI, Ozkan SA: **Boron-doped diamond electrodes: recent developments and advances in view of electrochemical drug sensors**. *Crit Rev Anal Chem* 2021:1–17, https://doi.org/10.1080/10408347.2020.1863769.

12. Sarakhman O, Švorc Ľ: **A review on recent advances in the applications of boron-doped diamond electrochemical sensors in food analysis**. *Crit Rev Anal Chem* 2020:1–23, https://doi.org/10.1080/10408347.2020.1828028.

13. Baluchová S, Daňhel A, Dejmková H, Ostatná V, Fojta M, Schwarzová-Pecková K: **Recent progress in the applications of boron doped diamond electrodes in electroanalysis of organic compounds and biomolecules – a review**. *Anal Chim Acta* 2019, **1077**:30–66, https://doi.org/10.1016/j.aca.2019.05.041.

14. Krečmarová M, Gulka M, Vandenryt T, Hrubý J, Fekete L, Hubík P, Taylor A, Mortet V, Thoelen R, Bourgeois E, Nesládek M: **A label-free diamond microfluidic DNA sensor based on active nitrogen-vacancy center charge state control**. *ACS Appl Mater Interfaces* 2021, **13**:18500–18510, https://doi.org/10.1021/acsami.1c01118.

15. Niedzialkowski P, Slepski P, Wysocka J, Chamier-Cieminska J, Burczyk L, Sobaszek M, Wcislo A, Ossowski T, Bogdanowicz R, Ryl J: **Multisine impedimetric probing of biocatalytic reactions for label-free detection of DEFB1 gene: how to verify that your dog is not human?** *Sens Actuators B Chem* 2020, **323**:128664, https://doi.org/10.1016/j.snb.2020.128664.

16. Muzyka K, Sun J, Fereja TH, Lan Y, Zhang W, Xu G: **Boron-doped diamond: current progress and challenges in view of electroanalytical applications**. *Anal Methods.* 2019, **11**:397–414, https://doi.org/10.1039/C8AY02197J.

17. Wang P, Yuan X, Cui Z, Xu C, Sun Z, Li J, Liu J, Tian Y, Li H: **A nanometer-sized graphite/boron-doped diamond electrochemical sensor for sensitive detection of acetaminophen**. *ACS Omega* 2021, **6**:6326–6334, https://doi.org/10.1021/acsomega.0c06141.

18. Yu S, Yang N, Liu S, Jiang X: **Electrochemical and photochemical CO_2 reduction using diamond**. *Carbon* 2021, **175**:440–453, https://doi.org/10.1016/j.carbon.2021.01.116.

19. * Wang J, Su Y, Tian Y, Xiang X, Zhang J, Li S, He D: **Porous single-crystal diamond**. *Carbon* 2021, **183**:259–266, https://doi.org/10.1016/j.carbon.2021.06.083.
Authors formed large diamond crystals dominated by the (111) facets using the HPHT growth driven by small nanocrystals adsorbed to larger seeds in a metal matrix that minimises their surficial energy.

20. ** Wood GF, Zvoriste-Walters CE, Munday MG, Newton ME, Shkirskiy V, Unwin PR, Macpherson JV: **High pressure high temperature synthesis of highly boron doped diamond microparticles and porous electrodes for electrochemical applications**. *Carbon* 2021, **171**:845–856, https://doi.org/10.1016/j.carbon.2020.09.038.
Report shows synthesis of boron-doped microparticles utilising AlB2 forming porous electroactive HPHT-compressed boron-doped particles ((111)-dominant planes) providing metal-like conductivity. The high-rate CVs were obtained at a resin-isolated (111)-faceted surface using a nanopipette.

21. * Wang J-C, Chen H, Wan L-F, Mu C-Y, Liu Y-F, Cheng S-H, Wang Q-L, Li L-A, Li H-D: **Ohmic and Schottky contacts of hydrogenated and oxygenated B-doped single crystal diamond with hill-like polycrystalline grains**. *Chin Phys B* 2021, https://doi.org/10.1088/1674-1056/ac032b.
The authors present the formation of nanoscaled Schottky contacts at hill-like polycrystalline diamond grains emerging at boron-doped single-crystal diamonds, emerging as a result of surface oxygen termination.

22. Gupta S, Evans B, Henson A, Carrizosa SB: **Salt-assisted ultrasonicated de-aggregation and advanced redox electrochemistry of detonation nanodiamond**. *Materials* 2017, **10**:1292, https://doi.org/10.3390/ma10111292.

23. Pleskov YuV, Krotova MD, Ekimov EA: **The compacts of boron-doped synthetic diamond: methods for the increasing of their electrochemical activity**. *J Electroanal Chem* 2021, **888**:115203, https://doi.org/10.1016/j.jelechem.2021.115203.

24. Wang H, Tzeng Y-K, Ji Y, Li Y, Li J, Zheng X, Yang A, Liu Y, Gong Y, Cai L, Li Y, Zhang X, Chen W, Liu B, Lu H, Melosh NA, Shen Z-X, Chan K, Tan T, Chu S, Cui Y: **Synergistic enhancement of electrocatalytic CO_2 reduction to C2 oxygenates at nitrogen-doped nanodiamonds/Cu interface**. *Nat Nanotechnol* 2020, **15**:131–137, https://doi.org/10.1038/s41565-019-0603-y.

25. * Piatti E, Pasquarelli A, Gonnelli RS: **Orientation-dependent electric transport and band filling in hole co-doped epitaxial diamond films**. *Appl Surf Sci* 2020, **528**:146795, https://doi.org/10.1016/j.apsusc.2020.146795.
The first-principles approach allowed for the atomic-scale understanding of the orientation and dopant concentration-dependent electronic band structure of boron-doped diamond surfaces observed as a variation of the energy-impacted electronic density of states.

26. Larsson K: **Simulation of diamond surface chemistry: reactivity and properties**. In *Some aspects of diamonds in scientific research and high technology*. Edited by Lipatov E, IntechOpen; 2020, https://doi.org/10.5772/intechopen.86865.

27. Liang Y, Pfisterer JHK, McLaughlin D, Csoklich C, Seidl L, Bandarenka AS, Schneider O: **Electrochemical scanning probe microscopies in electrocatalysis**. *Small Methods* 2019, **3**:1800387, https://doi.org/10.1002/smtd.201800387.

28. Zhou Y, Takahashi Y, Fukuma T, Matsue T: **Scanning electrochemical microscopy for biosurface imaging**. *Curr Opin Electrochem* 2021, **29**:100739, https://doi.org/10.1016/j.coelec.2021.100739.

29. Daboss S, Knittel P, Nebel CE, Kranz C: **Multifunctional boron-doped diamond colloidal AFM probes**. *Small* 2019, **15**:1902099, https://doi.org/10.1002/smll.201902099.

30. Gharbi O, Ngo K, Turmine M, Vivier V: **Local electrochemical impedance spectroscopy: a window into heterogeneous interfaces**. *Curr Opin Electrochem* 2020, **20**:1–7, https://doi.org/10.1016/j.coelec.2020.01.012.

31. Bentley CL: **Scanning electrochemical cell microscopy for the study of (nano)particle electrochemistry: from the sub-particle to ensemble level**. *Electrochem Sci Adv* 2021, https://doi.org/10.1002/elsa.202100081.

32. Zhao H, Ma J, Zuo X, Li F: **Electrochemical analysis for multiscale single entities on the confined interface†**. *Chin J Chem* 2021, **39**:1745–1752, https://doi.org/10.1002/cjoc.202000722.

33. Marinesco S: **Micro- and nano-electrodes for neurotransmitter monitoring**. *Curr Opin Electrochem* 2021, **29**:100746, https://doi.org/10.1016/j.coelec.2021.100746.

34. Knittel P, Yoshikawa T, Nebel CE: **Diamond colloidal probe force spectroscopy**. *Anal Chem* 2019, **91**:5537–5541, https://doi.org/10.1021/acs.analchem.9b00693.

35. Wang Y, Cao Z, Yang Q, Guo W, Su B: **Optical methods for studying local electrochemical reactions with spatial resolution: a critical review**. *Anal Chim Acta* 2019, **1074**:1–15, https://doi.org/10.1016/j.aca.2019.02.053.

36. Caniglia G, Kranz C: **Scanning electrochemical microscopy and its potential for studying biofilms and antimicrobial coatings**. *Anal Bioanal Chem* 2020, **412**:6133–6148, https://doi.org/10.1007/s00216-020-02782-7.

37. Henrotte O, Boudet A, Limani N, Bergonzo P, Zribi B, Scorsone E, Jousselme B, Cornut R: **Steady-state electrocatalytic activity evaluation with the redox competition mode of scanning electrochemical microscopy: a gold probe and a boron-doped diamond substrate**. *ChemElectroChem* 2020, **7**:4633–4640, https://doi.org/10.1002/celc.202001088.

38. Counihan MJ, Setwipatanachai W, Rodríguez-López J: **Interrogating the surface intermediates and water oxidation products of boron-doped diamond electrodes with scanning electrochemical microscopy**. *ChemElectroChem* 2019, **6**:3507–3515, https://doi.org/10.1002/celc.201900659.

39. ** Liu D, Chen C, Perry D, West G, Cobb SJ, Macpherson JV, Unwin PR: **Facet-resolved electrochemistry of polycrystalline boron-doped diamond electrodes: microscopic factors determining the solvent window in aqueous potassium chloride solutions**. *ChemElectroChem* 2018, **5**:3028–3035, https://doi.org/10.1002/celc.201800770.
The authors present a deep insight into the facet-resolved, electrochemical properties of polycrystalline BDD, locally determined by the boron dopant concentration and to less extent the surface termination type, valuable for designing electrodes with a tailored electrolytic window.

40. Zhai Z, Huang N, Yang B, Wang C, Liu L, Qiu J, Shi D, Yuan Z, Lu Z, Song H, Zhou M, Chen B, Jiang X: **Insight into the effect of the core–shell microstructure on the electrochemical properties of undoped 3D-networked conductive diamond/graphite**. *J Phys Chem C* 2019, **123**:6018–6029, https://doi.org/10.1021/acs.jpcc.8b11865.

41. Ryl J, Burczyk L, Zielinski A, Ficek M, Franczak A, Bogdanowicz R, Darowicki K: **Heterogeneous oxidation of highly boron-doped diamond electrodes and its influence on the surface distribution of electrochemical activity**. *Electrochim Acta* 2019, **297**:1018–1027, https://doi.org/10.1016/j.electacta.2018.12.050.

42. Ryl J, Cieslik M, Zielinski A, Ficek M, Dec B, Darowicki K, Bogdanowicz R: **High-temperature oxidation of heavy boron-doped diamond electrodes: microstructural and electrochemical performance modification**. *Materials* 2020, **13**:964, https://doi.org/10.3390/ma13040964.

43. Ivandini TA, Watanabe T, Matsui T, Ootani Y, Iizuka S, Toyoshima R, Kodama H, Kondoh H, Tateyama Y, Einaga Y: **Influence of surface orientation on electrochemical properties of boron-doped diamond**. *J Phys Chem C* 2019, **123**:5336–5344, https://doi.org/10.1021/acs.jpcc.8b10406.

44. Lourencao BC, Brocenschi RF, Medeiros RA, Fatibello-Filho O, Rocha-Filho RC: **Analytical applications of electrochemically pretreated boron-doped diamond electrodes**. *ChemElectroChem* 2020, **7**:1291–1311, https://doi.org/10.1002/celc.202000050.

45. Oturan MA: **Outstanding performances of the BDD film anode in electro-Fenton process: applications and comparative performance**. *Curr Opin Solid State Mater Sci* 2021, **25**:100925, https://doi.org/10.1016/j.cossms.2021.100925.

46. Martínez-Huitle CA, Brillas E: **A critical review over the electrochemical disinfection of bacteria in synthetic and real wastewaters using a boron-doped diamond anode**. *Curr Opin Solid State Mater Sci* 2021, **25**:100926, https://doi.org/10.1016/j.cossms.2021.100926.

47. Nidheesh PV, Divyapriya G, Oturan N, Trellu C, Oturan MA: **Environmental applications of boron-doped diamond electrodes: 1. Applications in water and wastewater treatment**. *ChemElectroChem* 2019, **6**:2124–2142, https://doi.org/10.1002/celc.201801876.

48. Martínez-Huitle CA, Panizza M: **Electrochemical oxidation of organic pollutants for wastewater treatment**. *Curr Opin Electrochem* 2018, **11**:62–71, https://doi.org/10.1016/j.coelec.2018.07.010.

49. Dettlaff A, Sobaszek M, Klimczuk T, Bogdanowicz R: **Enhanced electrochemical kinetics of highly-oriented (111)-textured boron-doped diamond electrodes induced by deuterium plasma chemistry**. *Carbon* 2021, **174**:594–604, https://doi.org/10.1016/j.carbon.2020.11.096.

50. Xu J, Yokota Y, Wong RA, Kim Y, Einaga Y: **Unusual electrochemical properties of low-doped boron-doped diamond electrodes containing sp^2 carbon**. *J Am Chem Soc* 2020, **142**:2310–2316, https://doi.org/10.1021/jacs.9b11183.

51. Baluchová S, Taylor A, Mortet V, Sedláková S, Klimša L, Kopeček J, Hák O, Schwarzová-Pecková K: **Porous boron doped diamond for dopamine sensing: effect of boron doping level on morphology and electrochemical performance**. *Electrochim Acta* 2019, **327**:135025, https://doi.org/10.1016/j.electacta.2019.135025.

52. Zhang J, Coffinier Y, Zhao Z-Y, Szunerits S, Barras A, Yu X, Boukherroub R: **Preparation of boron-doped diamond nanospikes on porous Ti substrate for high-performance supercapacitors**. *Electrochim Acta* 2020, **354**:136649, https://doi.org/10.1016/j.electacta.2020.136649.

53. Banerjee D, Sankaran KJ, Deshmukh S, Ficek M, Yeh C-J, Ryl J, Lin I-N, Bogdanowicz R, Kanjilal A, Haenen K, Sinha Roy S: **Single-step grown boron doped nanocrystalline diamond-carbon nanograss hybrid as an efficient supercapacitor electrode**. *Nanoscale* 2020, **12**:10117–10126, https://doi.org/10.1039/D0NR00230E.

54. Santos NF, Pereira SO, Fernandes AJS, Vasconcelos TL, Fung CM, Archanjo BS, Achete CA, Teixeira SR, Silva RF, Costa FM: **Physical structure and electrochemical response of diamond–graphite nanoplatelets: from CVD synthesis to label-free biosensors**. *ACS Appl Mater Interfaces* 2019, **11**: 8470–8482, https://doi.org/10.1021/acsami.9b00352.